PAPER

Supporting capacity of a ferrofluid ring bearing

View the article online for updates and enhancements.

Supporting capacity of a ferrofluid ring bearing

Xingfei Xie, Qingwen Dai[iD]**, Wei Huang**[iD] **and Xiaolei Wang**[iD]

National Key Laboratory of Science and Technology on Helicopter Transmission, Nanjing University of Aeronautics and Astronautics, Nanjing 210016, People's Republic of China

E-mail: huangwei@nuaa.edu.cn

CrossMark

Abstract

In this paper, the supporting capacity of a ferrofluids (FFs) ring bearing is investigated experimentally and numerically. The bearing consists of a floating plate, a substrate, and a FFs ring sandwiched between them. The FFs ring is formed and restrained by applying a ring magnet below the substrate. For a FFs ring with a thickness of 0.25 mm, the maximum supporting force is about 1.78 N. Numerical analysis reveals that, compared with the Laplace force, the magnetic force plays a dominating role in the total supporting force. Such a liquid ring support may give underlying applications for frictionless bearings or precision positioning systems.

Supplementary material for this article is available online

Keywords: ferrofluid bearing, liquid support, magnetic field, lubrication

(Some figures may appear in colour only in the online journal)

1. Introduction

Friction is everywhere, from the scale of tiny atoms [1] to the crustal plates [2]. It can be defined as the rubbing of one body against another. Except for some technical applications that pursue higher friction, it is usually undesirable. Non-contact fluid bearings, known as hydrodynamic or hydrostatic bearings, are the most important methods to reduce friction. For hydrodynamic bearings, the solid–solid contact is eliminated by the support of a pressurized lubricating film due to relative movement [3]. Irrespective of the motion, hydrostatic lubrication is the proper way and the pressure is generated by a hydraulic pump [4]. However, the constraints on pressurized film formation restrict the applications of these two bearings to some degree, especially in micro-precision machinery.

Recently, liquid bridge bearings have offered another way to provide liquid support [5–8]. Surface tension between the thin liquid film and the patterned hydrophobic/hydrophilic surfaces acts as the bearing mechanism [6]. As an example mentioned in [7], alternate hydrophobic and hydrophilic annular tracks were fabricated to produce free energy barriers on the surface of a solid (see figure 1(a)). Thus, the liquid can be anchored on the hydrophilic track, forming a liquid ring. When compressed, the Laplace pressure built in the liquid ring is significantly greater than the atmospheric pressure and can provide an extra load-carrying capacity. Made of a fluid, the liquid bridge bearing may, obviously, avoid the solid–solid contact and improve the motion precision and reliability. The bearing mechanism usually requires complicated processes to fabricate the qualified surfaces with alternant hydrophilic/hydrophobic structures. Questions then arise: is there any other method to locate the liquid? In addition, besides the Laplace pressure, can any other kind of pressure be formed in the liquid to further enhance the total supporting force?

Ferrofluids (FFs) are smart colloidal suspensions of single domain ferromagnetic nanoparticles dispersed in a liquid carrier [9]. To avoid agglomeration, the surface of the nanoparticles is decorated with a long-chained organic molecule. The behavior of FFs depends mostly on their magnetic properties. In the presence of an external magnetic field, such a fluid can be shaped and positioned at a desired area [10]. Meanwhile, due to the particle magnetization and pole orientation, an extra 'magnetic pressure' is formed in the fluid [11], which may generate a controllable supporting force. Then, for a liquid bridge bearing, the total load-carrying capacity will be
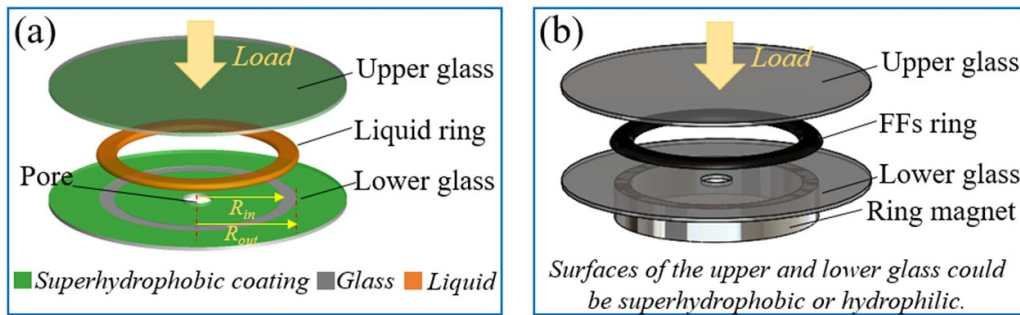
1

Figure 1. (a) Diagram of a liquid ring bearing and (b) a FFs ring bearing under a magnetic field.

expected to increase further when using field-induced FFs as a liquid medium.

In this paper, two groups of experiment were carried out. (a) The liquid bridge bearing capacities of water-based FFs and pure water on the patterned hydrophobic and hydrophilic surfaces were tested and compared. (b) On the superhydrophobic (or hydrophilic) surface, the bearing force of a FFs ring under a magnetic field was measured. Much attention was paid to the effect of the magnetic field. Meanwhile, numerical calculation was performed to better understand the performance of the axial FFs ring bearing.

2. Experimental details

The liquid bridge bearing contained two glass plates with the size of $\Phi 50 \times 0.5$ mm. The surfaces of the two glasses were sprayed with a commercial paint (NeverWet, Ross Technology Corp., USA) to form a superhydrophobic chemical coating (water contact angle $\sim 165°$). After that, a ring pattern of the coating with the inner radius $R_{in} = 10$ mm and outer radius $R_{out} = 12.5$ mm was removed by laser-marking technology. Due to the relatively high surface energy, the exposed ring surface of the glass was hydrophilic (water contact angle $\sim 37°$) and the rest was still superhydrophobic. The ring pattern was only fabricated on the lower glass surface, as illustrated in figure 1(a). To dispel the effect of atmospheric pressure, a pore was processed in the center of the lower glass to link the outside environment and the inside cavity of the liquid ring. As a certain volume of water was dropped on the hydrophilic surface, a liquid ring was formed due to the surface energy barrier at the border of the ring pattern. When compressed by the upper glass, the Laplace pressure inside the liquid may produce a supporting force.

Figure 1(b) shows a schematic drawing of a FFs bearing under a magnetic field. A ring magnet (N35 NdFeB, $\Phi 25$ mm $\times \Phi 20$ mm $\times 5$ mm) with the same inner and outer radius as the ring pattern (shown in figure 1(a)) was applied under the glass plate. The magnetic field strength on the ring surface was about 280 mT. When a drop of FFs was injected to the lower glass surface, due to the adsorption of the magnetic field, a closed FFs ring appeared on the glass surface. Similarly, such a FFs ring may also be expected to provide bearing capacity as a result of FFs magnetization. Here, two
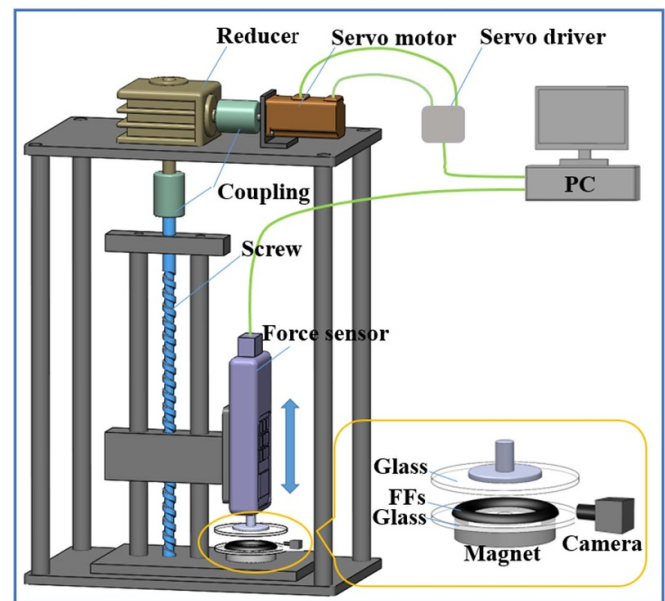

Figure 2. Diagram of the test system.

simple surfaces were applied: glass (hydrophilic) and glass covered with a superhydrophobic chemical coating (superhydrophobic).

Two kinds of supported liquid ring were tested by using a force-testing platform, as shown in figure 2. The upper glass plate fixed with a pull-press sensor shifted in a vertical direction at a speed of 0.008 mm s^{-1}. The range of the sensor was 5 N with a resolution of 0.001 N. Before the test, the lower glass was kept horizontal by using an air level. The upper one was covered on the surface of the lower glass. After that, the upper glass was fixed with the force sensor and moved up. In this way, the two glasses could be regarded as parallel. For each test, the dosage of the liquid (water or FFs) injected on the lower substrate was controlled at 0.2 ml. As the upper glass pressed on the fluid surface, the data of the liquid-bearing force over the axial displacement could be captured by a data-acquisition system. Meanwhile, the outline pictures of the FFs ring in a certain gap were taken using an industrial digital camera. Thus, the interfacial contact angles of the fluid on the upper and lower glasses could be obtained.

Table 1. Main properties of the ferrofluid.

Parameters	Value
Nanoparticles	Fe_3O_4
Particles diameter, d	10 ± 2 nm
Volume fraction of nanoparticles, $\emptyset_p$	4.3%
Density, ρ	1.2 g cm^{-3}
Dynamic viscosity, η	5 mPa·s
Surface tension, γ	32 mN m^{-1}
Saturation magnetization, M_s	1.52×10^4 A m^{-1}

For comparing with water, a commercial water-based FFs comprising Fe_3O_4 nanoparticles was chosen and the main properties of the fluid are shown in table 1. The contact angles of the fluid were measured using an industrial digital camera and the values were 152° and 19° on the superhydrophobic coating and hydrophilic glass surface, respectively.

3. Results and discussion

The supporting force of the liquid bridge bearing with an individual liquid ring between patterned glass surfaces, as depicted in figure 1(a), was tested and the result is shown in figure 3. The force of the liquid ring enhances gradually while the upper glass is moving down, and the maximum value reaches 0.13 N for a water ring with a thickness of 0.4 mm. As mentioned in [7], the supporting force mainly consists of two parts. One is the Laplace force, which originates from the Laplace pressure difference across the air/liquid interface and its direction is vertically upward. The other is the normal component of the capillary force, which assists to drag the upper and lower glasses together. Usually, this part is small enough to be ignored, but it deserves greater attention in microscale. Based on the Young–Laplace equation, the pressure difference across the liquid/air interface is $\Delta P_{\text{Lap}} = \gamma/R_C$, where γ is the surface tension of the liquid and R_C is the curvature radius of the air/liquid interface. R_C can be calculated as $1/(1/r + 1/R)$, where r is the curvature radius of the interface in the fluid cross-sectional plane, and R is the interfacial curvature radius in the horizontal plane of the ring. Actually, $R \gg r$, therefore $R_C \approx r_{\text{out}}$ or r_{in} (see figure 3). As the upper glass approaches the lower one, the R_C decreases gradually, which enhances the ΔP_{Lap} as well as the supporting force. Theoretically, the supporting force relies mainly on the limited contact angle of the fluid and the gap height of the two glasses.

It is interesting to find that the force fluctuates obviously when the height (h) is lower than 0.4 mm. Given the decreasing gap between the two glasses, the cross-sectional image of the liquid ring deforms gradually. When the liquid contact angle exceeds its critical value on the superhydrophobic coating, tiny droplets of the liquid may migrate from the ring bulk and the supporting force decreases rapidly. However, due to the surface tension, a new integrated ring is formed shortly afterwards. Accompanied by the decreasing height in the gap, the force enhances again. Because of the reduced volume of the total liquid, the bearing force declines obviously compared with the previous ring. The supporting behavior of the
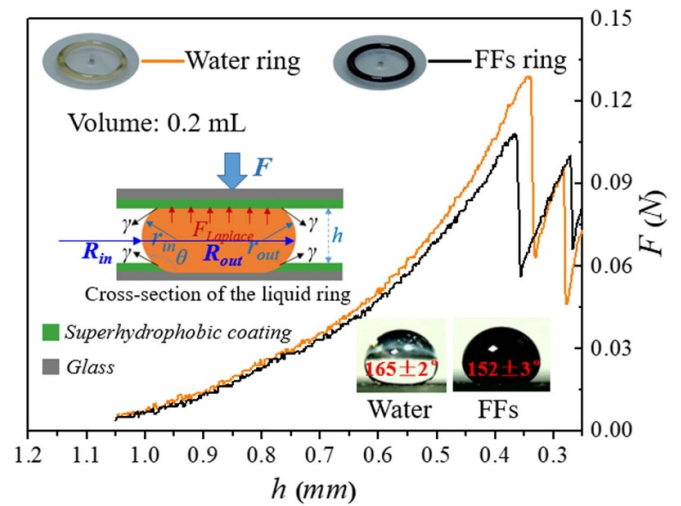

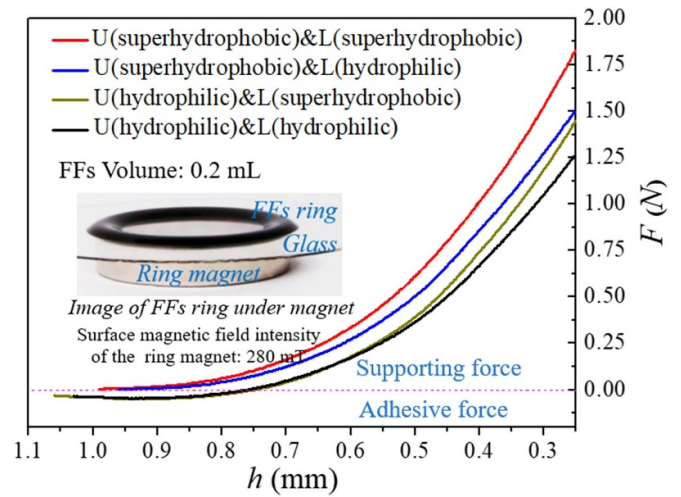**Figure 3.** Supporting force of the liquid ring between the patterned glass surfaces.

Figure 4. Supporting force of the FFs ring under a magnetic field.

water-based FFs ring presents the same variation tendency as the water ring. Compared with the FFs, pure water exhibits a higher contact angle. The differences in contact angle could be caused by two reasons. One is the difference in mass due to the different fluid density [12]. The other could be the lower surface tension of the FFs due to the existence of surfactant. As is known, to overcome particle agglomeration, a magnetic nanoparticle is usually decorated with a surfactant made of long-chained molecules [9]. Such molecules in carrier liquid could decrease the surface tension of the FFs to some extent. Thus, the water ring possesses a larger bearing capacity at the same gap height and its first decline also appears at less of a gap height in contrast with the FFs.

The supporting force of the FFs ring under a magnetic field, as depicted in figure 1(b), was measured and the result is given in figure 4. The wettability of the glass surface was taken into account. The maximum values of the force range from 1.25 to 1.78 N at the gap height of 0.25 mm in the four cases. The different starting positions come from the various initial
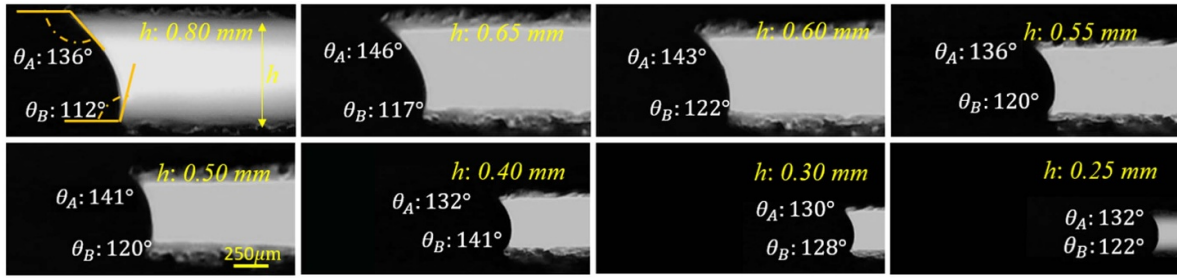
Figure 5. Cross-sectional views of the FFs outline under a magnetic field at different gap heights (FFs ring is between superhydrophobic surfaces).
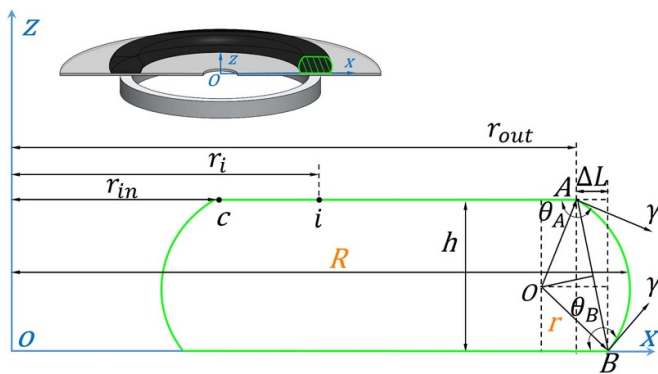

Figure 6. Geometrical model for an instantaneous cross-sectional view of the FFs ring between two glass plates.

shapes of the FFs ring. As the upper (U) glass is hydrophilic, the adhesive force appears at the very beginning whether the lower (L) glass is hydrophilic or hydrophobic. And the force transforms into a supporting one as the upper glass continues to move down. Provided that the upper glass is superhydrophobic, the FFs ring presents the supporting force all the time and the force is always higher than that when the upper glass is hydrophilic at the same gap height (h). The bearing capacity of the FFs ring between two superhydrophobic surfaces is the largest, while the lowest appears between hydrophilic surfaces. Overall, compared with the surface wettability, the effect of the magnetic field dominates the bearing capacity of the FFs ring.

Note that the maximum supporting force (1.25–1.78 N) of the four situations is about ten times the bearing capacity (0.13 N) of the liquid ring between patterned glass surfaces (see figure 3), although the same ring size and liquid volume are applied. It is known that each nanoparticle in FFs may be treated as a superparamagnetic nanoparticle suspended in a liquid carrier. Here, the liquid carrier of the FFs is water. In the presence of an external magnetic field, the original poles of these particles with random orientation will align in the direction of the external field. The interaction between the FFs and the magnetic field generates attractive force on each particle. The force on individual particles manifests itself as a magnetic body force [13] or 'magnetic pressure' [11] on the bulk of the FFs. This force can act

as an effective bearing capacity of the magnetized FFs ring. Generally, the magnetic force shows a linear relation with the external magnetic field intensity and gradient [14]. Due to the decreasing gap height, both the intensity and gradient of the magnetic field applied on the FFs become higher. As a result, the bearing capacity of the FFs ring continues to grow.

Meanwhile, the curve of the force keeps a steady growth even when the gap of the height (h) reaches 0.25 mm. No force fluctuatations are observed, which is quite different from the results shown in figure 3. As mentioned above, the force fluctuations of the liquid bridge bearing derive from the escape of the tiny liquid drops. Because of the existence of the magnetic field, FFs can always be restricted and positioned between the glass gap without mass loss. Therefore, the supporting force of the FFs ring is smoother and more controllable under a magnetic field.

To further understand the bearing mechanism, numerical calculation of the FFs ring under a magnetic field was conducted. For simplicity, the case of a FFs ring between two superhydrophobic surfaces was chosen. During the compressing process, the pictures of the FFs ring's outline at different h were taken using an industrial digital camera. The interfacial contact angles of the fluid on the upper and lower surface were obtained based on the collected pictures. As can be seen in figure 5, the outline of the FFs ring changes and the corresponding contact angles on the contact line also vary. Figure 6 shows a geometrical model of an instantaneous cross-sectional view of the FFs ring at a certain gap height.

In this model, the FFs supporting force with three aspects is taken into account. Similar to the liquid ring anchored on the hydrophilic track (see figures 1(a) and 3), the curved air/liquid interface creates the Laplace force (F_{Lap}), and the normal component of the capillary force (F_{γ}) is close to the air/liquid/solid contact line of the upper glass. The new addition is a magnetic force (F_{Mag}) caused by the external magnetic field. As mentioned above, during the magnetization process, the force on each magnetic particle transforms the bulk of the FFs.

As shown in figure 6, assuming the curvature radius r is equal, then it can be written as

$$r = \frac{h}{\cos(180° - \theta_{\text{A}}) + \cos(180° - \theta_{\text{B}})} \quad (1)$$

where h is the height of the FFs ring in the supporting gap, and θ_A and θ_B are the corresponding FFs interfacial contact angles on the upper and lower surfaces.

As mentioned above, the Laplace pressure between the inside of the fluid and the atmosphere is $\Delta P_{Lap} = \gamma/R_C$, where R_C is the curvature radius of the liquid/air interface. In figure 6, R_C can be calculated as $1/(1/r + 1/R)$, where r is the curvature radius of the liquid/air interface, and R is the curvature radius of the FFs ring in a horizontal plane. Due to the value of $r \ll R$, then $R_C \approx r$, and hence

$$\Delta P_{Lap} = \frac{\gamma}{R_C} = \frac{\gamma \left[\cos\left(180° - \theta_A\right) + \cos\left(180° - \theta_B\right)\right]}{h} \quad (2)$$

where γ is the surface tension of the FFs. The Laplace force (F_{Lap}) can be expressed as follows:

$$\begin{aligned} F_{Lap} &= \Delta P_{Lap} \pi (r_{out}^2 - r_{in}^2) \\ &= \frac{\pi\gamma\left[\cos\left(180° - \theta_A\right) + \cos\left(180° - \theta_B\right)\right]\left(r_{out}^2 - r_{in}^2\right)}{h}. \end{aligned} \quad (3)$$

To calculate the Laplace force (F_{Lap}), we should get the values of r_{in} and r_{out}, which are the radius of the inner and outer vertex of the FFs ring to the z axis. Since the volume of the FFs is constant, it can be approximately expressed as

$$V \approx \pi \left[(r_{out} + \Delta L)^2 - (r_{in} - \Delta L)^2 \right] h \quad (4)$$

where ΔL can be calculated from the following equation:

$$\Delta L = r\sin\left(180° - \theta_B\right) - r\sin\left(180° - \theta_A\right). \quad (5)$$

According to equation (4), one of the relations between r_{in} and r_{out} can be obtained. Meanwhile, due to the air pore in the center of the lower glass, the pressure of the inner FFs interface equals that of the outer (atmospheric pressure). Hence, the field intensity applied on the two interfaces (outer and inner) could be considered approximately equal, namely $H_{r_{in}} = H_{r_{out}}$. By using finite element software, at a certain height (h) above the lower glass, distributions of the magnetic field along the direction of the magnet's radius can be obtained. And the imported dimensional and magnetic parameters are consistent with the ring magnet ($\Phi 25$ mm $\times$ $\Phi 20$ mm $\times$ 5 mm, remanence B_r: 1.20 T and relative permeability μ_r: 1.1). As shown in figure 7, based on $H_{r_{in}} = H_{r_{out}}$, one more relation between r_{in} and r_{out} can be achieved. Combining equation (4), we can get the values of r_{in} and r_{out} at different gap heights, so that the Laplace force (F_{Lap}) of the FFs ring at a certain gap height can be calculated.

Then, the force induced by capillary force (F_γ) can be written as

$$F_\gamma = 2\pi\gamma\cos\left(\theta_A - 90°\right)\left(r_{out} + r_{in}\right) \quad (6)$$

where θ_A is the contact angle on the contact line (see figure 5). The direction of F_γ is vertically downward and it reduces the supporting force.
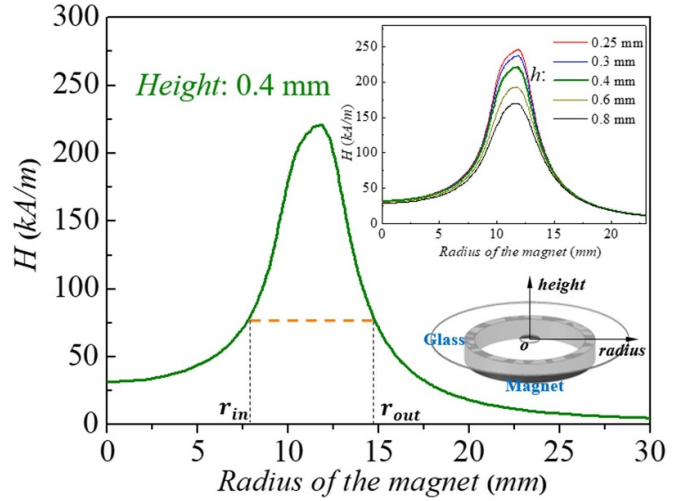

Figure 7. Distribution of magnetic field intensity at the height of 0.4 mm above the lower glass as a function of the magnet's radius (the inset shows the five different heights).

Next is to calculate the magnetic force. As shown in the geometrical model (see figure 6), under an external magnetic field, the pressure for points c (r_{in}) and i (r_i, any point on the upper surface) on the FFs based on Bernoulli's equation is given by [15]

$$P_{r_i} - \mu_0 \int_0^{H_{r_i}} M_H dH = P_{r_{in}} - \mu_0 \int_0^{H_{r_{in}}} M_H dH \quad (7)$$

where μ_0 is the space permeability and M_H is the magnetization of the FFs.

For ideal FFs with spherical nanoparticles, discarding the interaction between each particle, the magnetization of FFs can be determined by the Langevin equation [16]:

$$M_H = M_s L(\alpha) = M_s \left(\frac{e^{2\alpha} + 1}{e^{2\alpha} - 1} - \frac{1}{\alpha} \right) \quad (8)$$

where M_s (1.52×10^4 A m^{-1}) is the saturation magnetization of the FFs. α is the Langevin parameter and can be written as $\alpha = \mu_0 m_d H/(kT)$, where m_d is the magnetic moment of a nanoparticle, H is the external magnetic field, k is Boltzmann's constant, and T (300 K) is the absolute temperature.

The magnetic moment of a particle is $m_d = \frac{1}{6}M_d\pi d^3$, where d (10 nm) is the diameter of the particle. $M_d = M_s/\emptyset_p$ is the domain magnetization of solid particles. Here, $\emptyset_p$ (4.3%) is the volume fraction of the nanoparticles in the FFs.

So the magnetic pressure at any point of the FFs upper surface can be written as

$$P_{r_i} = P_{r_{in}} + \mu_0 \int_{H_{r_{in}}}^{H_{r_i}} M_H dH = P_{r_{in}} + \mu_0 M_s \int_{H_{r_{in}}}^{H_{r_i}} \frac{e^{2\alpha} + 1}{e^{2\alpha} - 1} - \frac{1}{\alpha} dH$$
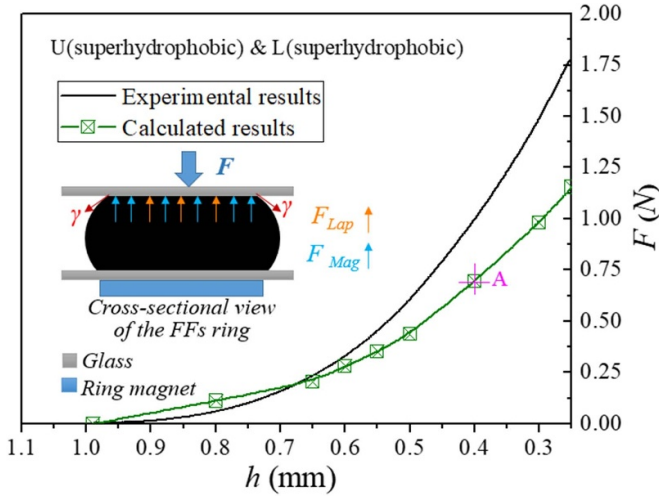
Figure 8. Calculated and experimental curves of the supporting force produced by the FFs ring between superhydrophobic surfaces.
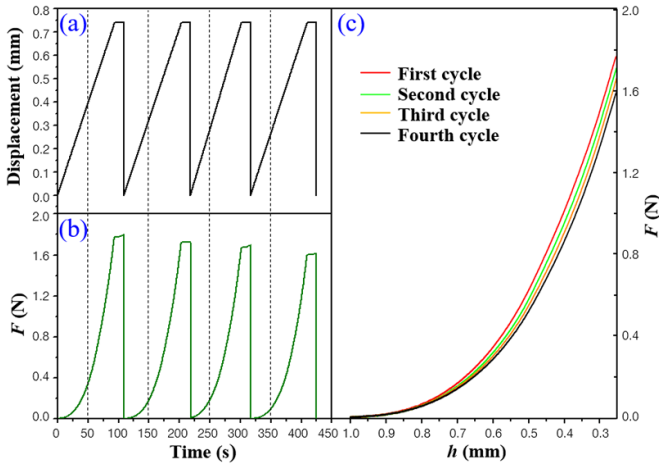

Figure 9. Multiple cycles supporting process of a FFs ring under a magnetic field between superhydrophobic surfaces: (a) four cycles of compression; (b) loading and unloading processes; (c) dynamic supporting force of each cycle.

$$
\begin{aligned}
&= P_{r_{\text{in}}} + \mu_0 M_s \left(\int_{H_{r_{\text{in}}}}^{H_{r_i}} \mathrm{d}H + \int_{H_{r_{\text{in}}}}^{H_{r_i}} \frac{2}{\mathrm{e}^{\frac{2\mu_0 m_d H}{kT}} - 1} \mathrm{d}H - \int_{H_{r_{\text{in}}}}^{H_{r_i}} \frac{kT}{\mu_0 m_d H} \mathrm{d}H \right) \\
&= P_{r_{\text{in}}} + \mu_0 M_s \left[\frac{kT}{\mu_0 m_d} \left(\ln \frac{\mathrm{e}^{\frac{2\mu_0 m_d H_{r_i}}{kT}} - 1}{\mathrm{e}^{\frac{2\mu_0 m_d H_{r_{\text{in}}}}{kT}} - 1} - \ln \frac{H_{r_i}}{H_{r_{\text{in}}}} \right) \right. \\
&\quad \left. - \left(H_{r_i} - H_{r_{\text{in}}} \right) \right].
\end{aligned} \tag{9}
$$

Once the pressure distribution (P_{r_i}) on the upper surface of the FFs ring is known, the magnetic force (F_{Mag}) can be calculated by integrating over the bearing surface

$$
F_{\text{Mag}} = \int_{r_{\text{in}}}^{r_{\text{out}}} P_{r_i} - P_{r_{\text{in}}} \mathrm{d}A
$$

$$
= 2\pi \mu_0 M_s \int_{r_{\text{in}}}^{r_{\text{out}}} \left[\frac{kT}{\mu_0 m_d} \left(\ln \frac{\mathrm{e}^{\frac{2\mu_0 m_d H_{r_i}}{kT}} - 1}{\mathrm{e}^{\frac{2\mu_0 m_d H_{r_{\text{in}}}}{kT}} - 1} - \ln \frac{H_{r_i}}{H_{r_{\text{in}}}} \right) \right.
$$

$$
\left. - \left(H_{r_i} - H_{r_{\text{in}}} \right) \right] r_i \mathrm{d}r. \tag{10}
$$

Thus, the total supporting force can be written as

$$
F_{\text{Supporting}} = F_{\text{Lap}} + F_{\text{Mag}} - F_\gamma. \tag{11}
$$

Combine equations (3), (6), (10), and (11), the total supporting force can be rearranged to become

$$
\begin{aligned}
F_{\text{Supporting}} &= F_{\text{Lap}} + F_{\text{Mag}} - F_\gamma \\
&= \frac{\pi\gamma \left[\cos\left(180° - \theta_A\right) + \cos\left(180° - \theta_B\right) \right] \left(r_{\text{out}}^2 - r_{\text{in}}^2 \right)}{h} \\
&\quad + 2\pi\mu_0 M_s \int_{r_{\text{in}}}^{r_{\text{out}}} \left[\frac{kT}{\mu_0 m_d} \left(\ln \frac{\mathrm{e}^{\frac{2\mu_0 m_d H_{r_i}}{kT}} - 1}{\mathrm{e}^{\frac{2\mu_0 m_d H_{r_{\text{in}}}}{kT}} - 1} - \ln \frac{H_{r_i}}{H_{r_{\text{in}}}} \right) \right. \\
&\quad \left. - \left(H_{r_i} - H_{r_{\text{in}}} \right) \right] r_i \mathrm{d}r - 2\pi\gamma \cos\left(\theta_A - 90°\right) \left(r_{\text{out}} + r_{\text{in}} \right).
\end{aligned} \tag{12}
$$

Figure 8 shows the calculated and experimental curves of the supporting forces produced by the FFs ring with a magnet. As can be seen, the theoretical results calculated by using equation (12) are in good agreement with the experimental data. Shown in figure 8 is a brief calculation example for point A. When the gap height between two glasses is 0.4 mm, the corresponding contact angles θ_A and θ_B are 132° and 141°, which can be obtained from the cross-sectional view of the FFs ring (see figure 5). According to equations (1) and (5), we can get $r = 0.277$ mm and $\Delta L = -0.03$ mm. Considering the constant volume of the FFs and the same magnetic field intensity at the positions of r_{in} and r_{out} (equation (4) and $H_{r_{\text{in}}} = H_{r_{\text{out}}}$), the values of $r_{\text{in}} = 7.71$ mm and $r_{\text{out}} = 14.85$ mm can be obtained. Then, based on figure 7, the value of $H_{r_{\text{in}}} = 73.35 \, \text{kA m}^{-1}$ can be achieved at the gap height of 0.4 mm. Now, the three forces $F_{\text{Lap}} = 0.059 \, \text{N}, F_{\text{Mag}} = 0.640 \, \text{N},$ and $F_\gamma = 0.003 \, \text{N}$ can be calculated, respectively. Thus, the total supporting force of the FFs ring is $F_{\text{Supporting}} = 0.696 \, \text{N}$. It seems that the magnetic force plays a dominant role in the total FFs supporting force. More detailed information about the calculation process and main physical parameters of FFs can be found in the supplementary material (available online at stacks.iop.org/JPD/54/175004/mmedia).

The above results manifest that FFs restricted on a superhydrophobic surface by an external magnetic field can produce a liquid supporting force. Next, in order to figure out the dynamic characteristics of the bearing capacity, the multiple cycles force test was performed. As shown in figure 9, four cycles of the load–unload process of the FFs ring under a magnetic field were operated between superhydrophobic surfaces. The maximum force of the first cycle is about 1.77 N, which is almost the same as the value shown in figure 8. The force curves of the four cycles remain consistent in general,

J. Phys. D: Appl. Phys. **54** (2021) 175004

X Xie *et al*

with good repeatability. Such a result confirms that the bearing capacity of the FFs ring under a magnetic field has good repeatability and dynamic performance. Besides, the axial FFs bearing has an adaptive loading property so long as the load is lower than the limited supporting capacity. As shown in figure 9(c), a slight drop of the maximum force is observed, which may be caused by the evaporation of the carrier liquid (water). As is known, at a certain gap height, the supporting area of the liquid will reduce during the volatilizing process. Thus, the total supporting force decreases slightly. To eliminate the issue, FFs with low-volatile carrier liquid should be chosen.

4. Conclusions

In this paper, the bearing force of FFs under a magnetic field was measured and the force was compared with the water bridge bearing. Numerical calculation was carried out to better understand the behavior of the axial ring bearing stack. The results show that, either on hydrophilic or superhydrophobic surfaces, FFs can be confined at desired places with the aid of a magnetic field. This may produce a controllable liquid supporting force, which is at least one order of magnitude higher than that of the liquid bridge bearing with the same dimension. Numerical analysis further confirms that, by comparison of the Laplace force, the magnetic force plays a dominating contribution in the total FFs support. This work gives new thought to liquid supporting, both static and dynamic, for applications that require frictionless bearing or high-precision positions.

Acknowledgment

ORCID iDs

Qingwen Dai ⬦ https://orcid.org/0000-0001-7422-4259
Wei Huang ⬦ https://orcid.org/0000-0002-8871-634X
Xiaolei Wang ⬦ https://orcid.org/0000-0002-9055-1011

References

[1] Mo Y, Turner K T and Szlufarska I 2009 Friction laws at the nanoscale *Nature* **457** 1116–19
[2] Scholz C H 1998 Earthquakes and friction laws *Nature* **391** 37–42
[3] Andablo-Reyes E, de Vicente J, Hidalgo-Álvarez R, Myant C, Reddyhoff T and Spikes H A 2010 Soft elasto-hydrodynamic lubrication *Tribol. Lett.* **39** 109–14
[4] Urreta H, Aguirre G, Kuzhir P and Lopez de Lacalle L N 2019 Actively lubricated hybrid journal bearings based on magnetic fluids for high-precision spindles of machine tools *J. Intell. Mater. Syst. Struct.* **30** 2257–71
[5] Chan M L, Yoxall B, Park H, Kang Z, Izyumin I, Chou J, Megens M M, Wu M C, Boser B E and Horsley D A 2012 Design and characterization of MEMS micromotor supported on low friction liquid bearing *Sensors Actuators* A **177** 1–9
[6] Sun G, Liu T, Sen P, Shen W, Gudeman C and Kim C-J 2014 Electrostatic side-drive rotary stage on liquid-ring bearing *J. Microelectromech. Syst.* **23** 147–56
[7] Wen J, Dini D and Reddyhoff T 2020 Design and optimization of a liquid ring thrust bearing *Tribol. Int.* **149** 105588
[8] Wen J, Reddyhoff T, Hu S, Puhan D and Dini D 2020 Exploiting air cushion effects to optimise a superhydrophobic/hydrophilic patterned liquid ring sealed air bearing *Tribol. Int.* **144** 106129
[9] Odenbach S 2003 Ferrofluids—magnetically controlled suspensions *Colloids Surf.* A **217** 171–8
[10] Huang W, Shen C, Liao S and Wang X 2010 Study on the ferrofluid lubrication with an external magnetic field *Tribol. Lett.* **41** 145–51
[11] Rosensweig R E 1985 *Ferrohydrodynamics* (Cambridge: Cambridge University Press)
[12] Latikka M, Backholm M, Timonen J V I and Ras R H A 2018 Wetting of ferrofluids: phenomena and control *Curr. Opin. Colloid Interface Sci.* **36** 118–29
[13] Oldenburg C, Borglin S E and Moridis G J 2000 Numerical simulation of ferrofluid flow for subsurface environmental engineering applications *Transp. Porous Med.* **38** 319–44
[14] Hu Z, Dai Q, Huang W and Wang X 2020 Liquid–gas support and lubrication based on a ferrofluid seal *J. Appl. Phys.* **53** 025002
[15] Bashtovoi V, Bossis G, Kuzhir P and Reks A 2005 Magnetic field effect on capillary rise of magnetic fluids *J. Magn. Magn. Mater.* **289** 376–8
[16] Vekas L, Rasa M and Bica D 2000 Physical properties of magnetic fluids and nanoparticles from magnetic and magneto-rheological measurements *J. Colloid Interface Sci.* **231** 247–54